THE ASTROPHYSICAL JOURNAL, 595:L69–L76, 2003 October 1

RHESSI OBSERVATIONS OF PARTICLE ACCELERATION AND ENERGY RELEASE IN AN INTENSE SOLAR GAMMA-RAY LINE FLARE

R. P. LIN,[1,2] S. KRUCKER,[1] G. J. HURFORD,[1] D. M. SMITH,[1,3] H. S. HUDSON,[1] G. D. HOLMAN,[4] R. A. SCHWARTZ,[4] B. R. DENNIS,[4] G. H. SHARE,[5] R. J. MURPHY,[5] A. G. EMSLIE,[6] C. JOHNS-KRULL,[7] AND N. VILMER[8]

Received 2003 June 17; accepted 2003 August 5; published 2003 September 8

ABSTRACT

We summarize *Reuven Ramaty High Energy Solar Spectroscopic Imager* (*RHESSI*) hard X-ray (HXR) and γ-ray imaging and spectroscopy observations of the intense (X4.8) γ-ray line flare of 2002 July 23. In the initial rise, a new type of coronal HXR source dominates that has a steep double–power-law X-ray spectrum and no evidence of thermal emission above 10 keV, indicating substantial electron acceleration to tens of keV early in the flare. In the subsequent impulsive phase, three footpoint sources with much flatter double–power-law HXR spectra appear, together with a coronal superhot ($T \sim 40$ MK) thermal source. The north footpoint and the coronal source both move systematically to the north-northeast at speeds up to $\sim$50 km s^{-1}. This footpoint's HXR flux varies approximately with its speed, consistent with magnetic reconnection models, provided the rate of electron acceleration varies with the reconnection rate. The other footpoints show similar temporal variations but do not move systematically, contrary to simple reconnection models. The γ-ray line and continuum emissions show that ions and electrons are accelerated to tens of MeV during the impulsive phase. The prompt de-excitation γ-ray lines of Fe, Mg, Si, Ne, C, and O—resolved here for the first time—show mass-dependent redshifts of 0.1%–0.8%, implying a downward motion of accelerated protons and α-particles along magnetic field lines that are tilted toward the Earth by $\sim$40°. For the first time, the positron annihilation line is resolved, and the detailed high-resolution measurements are obtained for the neutron-capture line. The first ever solar γ-ray line and continuum imaging shows that the source locations for the relativistic electron bremsstrahlung overlap the 50–100 keV HXR sources, implying that electrons of all energies are accelerated in the same region. The centroid of the ion-produced 2.223 MeV neutron-capture line emission, however, is located $\sim 20'' \pm 6''$ away, implying that the acceleration and/or propagation of the ions must differ from that of the electrons. Assuming that Coulomb collisions dominate the energetic electron and ion energy losses (thick target), we estimate that a minimum of $\sim 2 \times 10^{31}$ ergs is released in accelerated $>\sim$20 keV electrons during the rise phase, with $\sim 10^{31}$ ergs in ions above 2.5 MeV nucleon^{-1} and about the same in electrons above 30 keV released in the impulsive phase. Much more energy could be in accelerated particles if their spectra extend to lower energies.

Subject headings: acceleration of particles — Sun: flares — Sun: X-rays, gamma rays

1. INTRODUCTION

The Sun is the most energetic particle accelerator in the solar system, producing ions of up to tens of GeV and electrons of up to tens of MeV. Large solar flares are the most powerful explosions in the solar system, releasing up to $\sim 10^{32}$–10^{33} ergs in $\sim 10^2$–10^3 s. The accelerated 20–100 keV electrons (Lin & Hudson 1976) and the sometimes greater than $\sim$1 MeV nucleon^{-1} ions (Ramaty et al. 1995) appear to contain $\sim$10%–50% of this energy, indicating that the particle acceleration and energy release processes are intimately linked. Flare-accelerated electrons and ions colliding with the ambient solar atmosphere produce bremsstrahlung hard X-ray (HXR)/γ-ray continuum and γ-ray line emission, respectively. The NASA *Reuven Ramaty High Energy Solar Spectroscopic Imager* (*RHESSI*) mission (Lin et al. 2002), launched on 2002 February 5, provides high-resolution imaging and spectroscopy from soft X-rays to γ-rays. This issue presents *RHESSI* observations of the intense solar flare of 2002 July 23, including the first detailed HXR imaging spectroscopy, the first high-resolution spectroscopy of solar γ-ray lines, the first imaging above 100 keV, and the first imaging of solar γ-ray lines.

2. EXPERIMENTAL DETAILS

Since focusing optics are not presently feasible for HXRs and γ-rays, then the only viable method of obtaining arcsecond-class images is with Fourier transform imaging (Makashima et al. 1978; Kosugi et al. 1991). *RHESSI* (Hurford et al. 2002) is made up of nine bi-grid rotating modulation collimators (RMCs), each consisting of a pair of widely separated grids mounted on a rotating spacecraft, to provide a spatial resolution of 2.″3–3′ over the full-Sun ($\sim$1°) field of view. Behind each RMC is a coaxial germanium detector (GeD). As the spacecraft rotates ($\sim$15 revolutons per minute), the RMCs convert the spatial information from the source into the temporal modulation of the photon counting rates of the GeDs.

The GeDs (Smith et al. 2002) are cooled to less than $\sim$75 K to achieve a spectral resolution of $\sim$1 keV FWHM for HXRs,

[1] Space Sciences Laboratory, University of California at Berkeley, Grizzly Peak at Centennial Drive, Berkeley, CA 94720-3411; rlin@ssl.ssl.berkeley.edu, krucker@ssl.berkeley.edu, ghurford@ssl.berkeley.edu, dsmith@ssl.berkeley.edu, hhudson@ssl.berkeley.edu.

[2] Also at Department of Physics, University of California at Berkeley, 366 LeConte Hall, Berkeley, CA 94720-7300.

[3] Now at the Department of Physics and Santa Cruz Institute for Particle Physics, University of California at Santa Cruz, 1156 High Street, Santa Cruz, CA 95064.

[4] NASA Goddard Space Flight Center, Greenbelt, MD 20771; holman@nasa.gov, richard.schwartz@gsfc.nasa.gov, brian.r.dennis.1@nasa.gov.

[5] Naval Research Laboratory, 4555 Overlook Avenue, SW, Code 7600A, Washington, DC 20375-5352; share@osse.nrl.navy.mil, murphy@osse.nrl.navy.mil.

[6] Department of Physics, The University of Alabama in Huntsville, Huntsville, AL 35899; emslieg@email.uah.edu.

[7] Department of Physics and Astronomy, Rice University, MS 61, 6100 South Main, Houston, TX 77005-1892; cmj@rice.edu.

[8] LESIA, Observatoire de Paris, 5 Place Jules Janssen, 92195 Meudon Cedex, France; nicole.vilmer@obspm.fr.

increasing to ~4 keV FWHM at ~2 MeV, the best ever achieved for solar measurements. The GeDs are segmented into a thin (~1.5 cm thick) front segment that stops photons from soft X-rays (3 keV) up to ~300 keV and a thick rear segment (~7 cm) for ~300 keV–17 MeV photons, allowing the γ-ray spectrum to be measured with low dead time, even in the presence of the intense X-ray fluxes. When the count rates exceed preset thresholds, a thin (~10 keV cutoff) shutter (which is in throughout this flare) and a thick one (~15 keV cutoff) are inserted automatically in front of the GeDs to attenuate low-energy fluxes. The electronics are designed to eliminate pulse pileup, but in very intense flares, such as the one on 2002 July 2003, that have steep spectra and count rates exceeding 10^4 counts s^{-1} per detector, spectral distortions can still be significant.

3. OVERVIEW OF FLARE

The intense (*GOES* class X4.8, optical importance 2B) 2002 July 23 solar flare began at ~0018 UT in NOAA Active Region 0039 at S13°, E72° (NOAA Solar-Geophysical Data). The Hα, microwave radio, and HXR emissions all peaked at ~0028–0031 UT, with *GOES* soft X-rays peaking later, at 0035 UT. Starting at ~0025 UT, type III radio bursts were detected by ground-based observatories and by the *Wind* spacecraft, followed by type II and IV emission. An associated fast (2180 km s^{-1}) and wide coronal mass ejection was observed by the Large Angle and Spectrometric Coronagraph on the *Solar and Heliospheric Observatory* (*SOHO*) spacecraft, but no solar energetic particle event was detected in the interplanetary medium. For at least an hour before the flare, the Nobeyama Radioheliograph observed a large elongated loop structure extending ~80″ to the northeast, at both 17 and 34 GHz (White et al. 2003). This emission is consistent with an optically thin thermal source, but it is not observed by the *Transiton Region and Coronal Explorer* (*TRACE*) at 195 Å, suggesting it is hotter than ~1.5 MK. At the base of this loop, a bright compact source is detected at 17 GHz but not at 34 GHz, implying nonthermal emission.

The *RHESSI* flare HXR and γ-ray observations (Fig. 1) divide naturally into a rise phase (from ~0018 to ~0027 UT) dominated by a coronal HXR source that appears to be nonthermal, an impulsive phase (from ~0027 to ~0043 UT) with continuum and γ-ray line emission extending up to greater than ~7 MeV, and a decay phase (>~0043 UT) dominated by a superhot (~40 MK) thermal source (but with an HXR burst at ~0050 UT). *RHESSI*'s high spectral resolution and coverage down to low energies allow detailed measurements of the thermal/nonthermal transition. For this flare, the spatially integrated HXR spectra of up to ~300 keV, determined every 20 s, have been forward-fitted with a model consisting of an isothermal plasma component plus a double–power-law nonthermal electron component at high energies (Holman et al. 2003). The spatial distribution of HXR sources (Krucker, Hurford, & Lin 2003) is shown superposed on *TRACE* 195 Å images, together with the simultaneous spatially integrated X-ray spectra, in a movie.[9]

4. RISE PHASE

The *RHESSI* 12–20 keV and *GOES* 0.5–4 Å channels rise above the background at ~0018 UT. The HXR emission above 10 keV is concentrated in a coronal source about 22″ in diameter located 880″–890″ east, 240″–250″ south

[9] Available at http://hesperia.gsfc.nasa.gov/hessi/presentations/video.

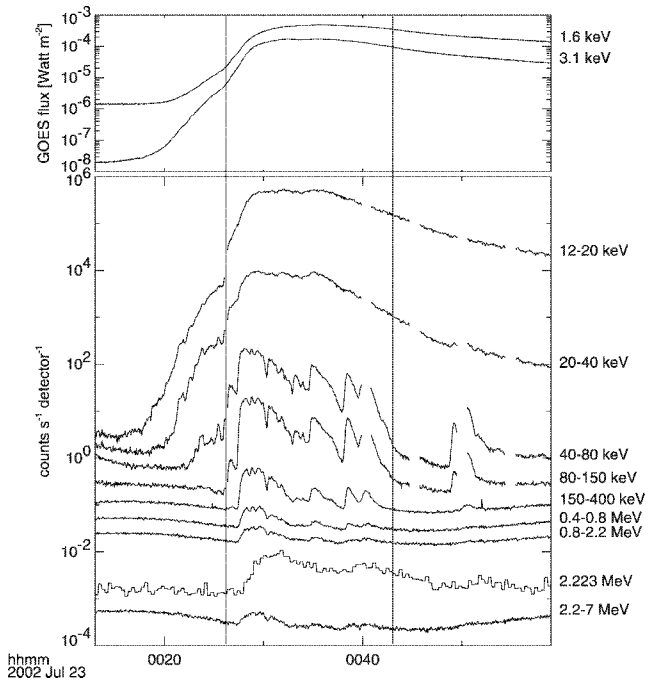

FIG. 1.—*RHESSI* HXR and γ-ray count rates (in units of counts s^{-1} per detector) for the 2002 July 23 flare, scaled to fit: 20–40 keV × 0.3; 40–80 keV × 0.07; 80–150 keV × 0.02; 150–400 keV; 400–800 keV × 0.001; 800–2218 keV × 0.0005; 2218–2228 keV × 0.01; and 2228–7000 keV × 2×10^{-5}. The thick shutter is inserted at ~0026, 0041, 0044, and 0050 UT and removed at ~0040, 0043, and 0049 UT. The slow variation through the interval is due to the background from cosmic-ray interactions with the atmosphere and spacecraft.

(Fig. 2, *top left*), about where the preflare compact 17 GHz radio source was located. This source generally has no chromospheric counterpart observed in *TRACE* 195 Å, *SOHO* Michelson Doppler Imager (MDI) white-light, or Hα images (Krucker et al. 2003). Brightenings in 195 Å emission (also in Hα) are detected along three approximately north-south aligned flare ribbons, located ~40″, ~10″, and ~20″ west of the coronal HXR source, beginning at ~0021, 0023, and 0024 UT, respectively. Some >10 keV HXR emission is detected sporadically from these ribbons, but it is always weaker than the coronal source.

The HXR spectra (Fig. 2, *top right*) are fitted to a double–power-law shape, with exponents of typically $\gamma_L \sim 5$ below and $\gamma_H \sim 6.5$ above a relatively sharp break at energies varying from $E_b \sim 20$ to ~35 keV. This clearly does not fit to an isothermal spectrum, although, in principle, a distribution of thermal sources with a range of temperatures might be able to reproduce the double–power-law spectral shape. Such a break can be produced if the electrons stop in a nonuniformly ionized target (Brown, Emslie, & Kontar 2003; Kontar, Brown, & McArthur 2002). Since this source is mostly confined to the ionized corona, the observed break must be intrinsic to the accelerated electron spectrum.

In the rise phase before 0026:08 UT, there is no spectral evidence of a thermal component above 10 keV. Assuming thick-target emission in a cold ambient medium ($E_e \gg kT$), the energy deposited by the electrons above ~10 keV, integrating over time from the rise to ~0026 UT, is estimated (Lin & Hudson 1976) to be greater than $\sim 4 \times 10^{32}$ ergs. By making the ad hoc assumption that a hot thermal plasma is present and by choosing the highest low-energy cutoff (~20 keV) that still fits the data, Holman et al. (2003) obtain a lower limit to the

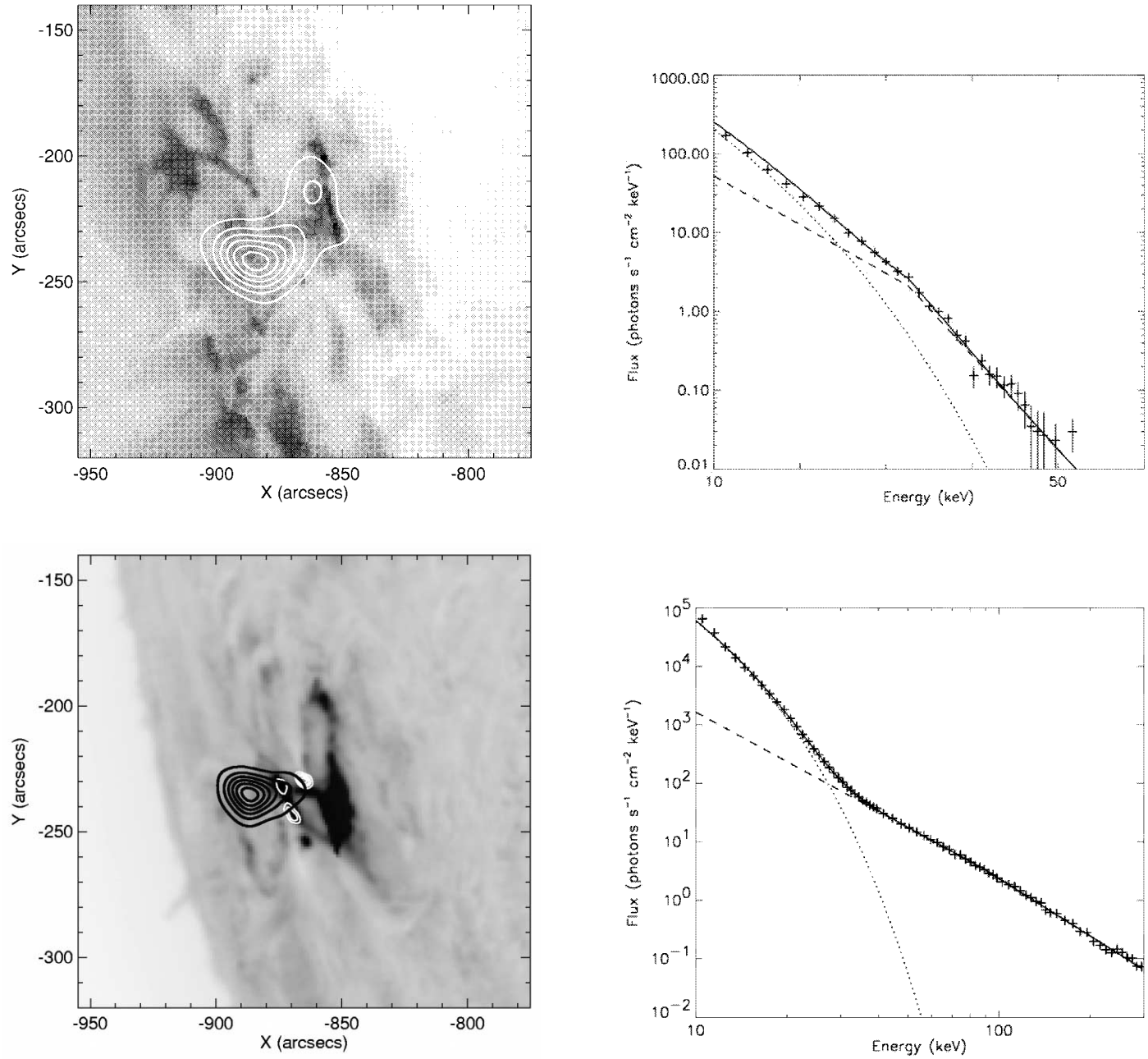

FIG. 2.—*Top left*: *RHESSI* 12–30 keV image (contour levels 15%, 30%, 45%, 60%, 75%, and 90%) during the rise phase (0021:42 UT) superposed on the *TRACE* 195 Å image. *Top right*: *RHESSI* X-ray spectrum for 0021:42 UT, with fit to isothermal (*dotted line*) and double–power-law (*dashed line*) spectra and the sum (*solid line*). *Bottom left*: *RHESSI* image (*black contours*: 12–18 keV, levels 15%, 30%, 45%, 60%, 75%, and 90%; *white contours*: 30–80 keV, levels 30%, 60%, 70%, and 90%) at 0028:15 UT during the impulsive phase, superposed on an Hα image from Big Bear Solar Observatory. *Bottom right*: *RHESSI* X-ray spectrum for 0028:15 UT, with fits as in the top right panel.

energy released in nonthermal electrons of $\sim 2 \times 10^{31}$ ergs. Since only a small fraction of the HXR emission is observed from footpoints along the *TRACE* ribbons, most of the energetic electron energy appears to be deposited into the coronal source.

The *GOES* soft X-ray time profile during the rise phase is similar to the time integral of the *RHESSI* HXR (12–25 keV) flux (i.e., the "Neupert" effect; Neupert 1968)—consistent with the energetic electrons colliding with the dense solar chromosphere in the footpoints, heating and evaporating the gas to form the high-temperature plasma. The *GOES* measurements at 0026 UT fit to a temperature of ~19 MK and an emission measure of 1.6×10^{49} cm^{-3}. Assuming that the *GOES* source is cospatial with the *RHESSI* HXR source (soft X-ray imaging is not available), whose volume is $V = \sim 4 \times 10^{27}$ cm^3, corresponding to $\sim$(22 arcsec)^3, we obtain a thermal plasma density of $\sim 6 \times 10^{10}$ cm^{-3} and an energy content in the soft X-ray plasma of only $\sim 10^{30}$ ergs, much less than the integral of the nonthermal electron energy over time. Even assuming that the *GOES* thermal source volume is 10 times larger only increases the thermal energy to $\sim 3 \times 10^{30}$ ergs.

For an ambient density of $\sim 6 \times 10^{10}$ cm^{-3}, the density of nonthermal electrons is $\sim 6 \times 10^{7}$ cm^{-3} (Holman et al. 2003), and the *e*-folding energy-loss time for 20–100 keV electrons is ~0.05–0.5 s (Lin 1974), implying that the primary flare energy release during the rise phase is going into accelerating electrons to continuously replenish the coronal source.

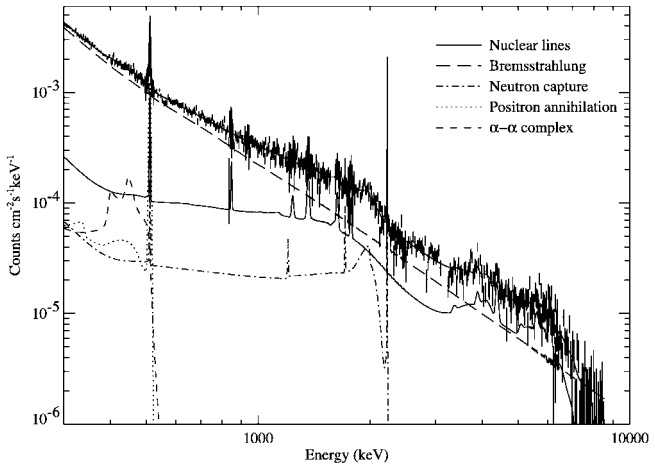

FIG. 3.—*RHESSI* γ-ray count spectrum from 0.3 to 10 MeV, integrated over the interval 0027:20–0043:20 UT. The lines show the different components of the model used to fit the spectrum.

5. IMPULSIVE PHASE

At ~0026:15 UT, there is an abrupt increase in the HXR emission and a change in its character; the thick shutter is inserted at this time. A "superhot" (~40 MK) thermal spectrum begins to dominate below ~30 keV (Fig. 2, *bottom right*). At the same time, the centroid of the 12–30 keV source shifts to the northeast by ~6″, suggesting that this superhot source is not cospatial with the rise-phase coronal nonthermal source (Fig. 2, *bottom left*). By ~0027:30 UT when the centroid of the coronal source is at 887″ east, 235″ south, strong emission is observed in three footpoints—north (initial centroid 866″ east, 230″ south from Sun center), south (869″ east, 243″ south), and middle (873″ east, 233″ south)—each with a chromospheric counterpart observed in Hα, EUV (*TRACE*), and white light (*SOHO* MDI; Krucker et al. 2003). The spatially integrated X-ray spectra (Fig. 2, *bottom right*), although still a double power law above ~30 keV, are much harder (HXR γ_L and $\gamma_H \sim$ 2.5–3.5) than those of the rise-phase coronal source, with typical break energies from ~70 to greater than 100 keV (Holman et al. 2003).

The north and south footpoints are located in an opposite polarity magnetic field (from the *SOHO* MDI magnetograph), separated by ~13″ (~10,000 km). Krucker et al. (2003) found that the temporal variations of the X-ray fluxes of these two footpoints track each other closely in time, to within seconds over the impulsive phase (to 00:40 UT), suggesting that they are at opposite ends of the same magnetic loops. During the first (and most intense) burst, the north footpoint rapidly moves north-northeast, roughly parallel to the magnetic neutral line, at speeds of up to ~50 km s^{-1}. The motions are only apparent; the HXR emission is shifting to the adjacent footpoints of newly reconnected field lines. The intensity of the north footpoint's HXR emission is observed generally to vary with its speed (Krucker et al. 2003). These observations indicate that magnetic reconnection is occurring in the corona, forming new magnetic loops that join the north and south footpoints. The speed of the footpoint varies as the rate of reconnection if the magnetic field strength is roughly constant. The rate of electron acceleration appears to vary with the rate of reconnection.

The superhot coronal source also moves in the same direction with a comparable speed (Krucker et al. 2003). Initially, the superhot source appears to exhibit the Neupert effect. After ~0029 UT, however, its intensity stays nearly constant, through the next burst at 0031 UT. The coronal source location (~20″ east of the north and south footpoints, which themselves are only separated by ~13″) suggests that it may be above the loop connecting these two footpoints, in the cusp formed by just reconnected field lines. Thus, the superhot source may be due to heating by the reconnection jets.

Although these general features support the reconnection picture, there are many puzzling details that indicate a much more complicated picture (see also Fletcher & Hudson 2002). The south footpoint and the middle footpoint (same polarity) stay nearly stationary with occasional abrupt jumps. The HXR flux of the middle footpoint only varies with the north footpoint until 00:30:30 UT, and its HXR emission disappears after ~00:32:30 UT. Furthermore, in both the first impulsive burst (~0027:30–0030 UT) and the second (0034:30–0037 UT), the north footpoint's HXR flux peaks before the speed reaches its maximum (Krucker et al. 2003).

HXR spectra obtained separately for the north, south, and middle footpoint sources (Emslie et al. 2003) were fitted to single X-ray power laws above ~50 keV (to avoid pulse-pileup effects not yet corrected for the individual sources). The power-law exponents of the north and south footpoints show the same temporal variations through most of the impulsive phase, but with the north footpoint's exponent being systematically ~0.3–0.4 larger. This difference could be the result of the acceleration mechanism, or it may indicate that the column density from the common accelerated electron source to the south footpoint is greater by a factor of ~1.5–2 than to the north source, so that Coulomb collisions will harden the electron spectrum by a greater amount in the south than in the north. The difference in column density could be due to the location of the acceleration region farther from the south source, a greater density in the leg of the loop toward the south source, or a larger pitch angle for the electrons streaming toward the south source. The middle source begins with the same spectral exponent as the north source but then becomes ~0.3–0.4 greater. If it is also linked magnetically to the north source, the difference in spectral index might be accounted for in a similar way.

6. GAMMA-RAY LINE EMISSION

Flare-accelerated protons and α-particles colliding with ambient carbon and heavier nuclei produce narrow prompt de-excitation lines (with widths of approximately a few keV to ~100 keV), while accelerated heavy nuclei colliding with ambient hydrogen and helium produce much broader lines that merge together to form a nuclear "continuum" (Ramaty & Murphy 1987). The collisions also produce neutrons, positrons, and pions. Neutron capture on hydrogen and positron annihilation yield narrow lines at 2.223 and 0.511 MeV, respectively, both of which are delayed. Gamma-ray line emission has been detected from many large solar flares (Chupp 1990; Share & Murphy 1995; Share et al. 2002). In this flare, the γ-ray line emission occurred predominantly during the impulsive phase (0027–0040 UT). Figure 3 shows the background-subtracted ~0.3–10 MeV γ-ray count spectrum, integrated over this time interval, with a preliminary fit to the bremsstrahlung continuum, narrow and broad prompt de-excitation γ-ray lines, the delayed neutron capture and positron annihilation lines, and the α-α lines—taking into account the full instrument response matrix including the off-diagonal elements.

The narrow prompt de-excitation lines of Fe, Mg, Si, Ne, C, and O are resolved for the first time (Smith et al. 2003). The line centroids exhibited significant Doppler redshifts from

~0.1% to 0.8%, and line widths of 0.1%–2.1% (FWHM) were measured. Both these quantities generally decrease with the mass of the emitting nucleus, as expected, since heavier nuclei will recoil less from a collision with a fast proton or α-particle. The redshifts, however, are too large for ions traveling downward in a radial magnetic field at the optical flare location. Assuming a model of accelerated ions with an isotropic distribution in the downward hemisphere along the magnetic field, the best fit gives a field direction tilted by ~40° from radial, toward the observer. For a narrow beam, the field could be nearly radial, but *RHESSI*'s measurement of the γ-ray line complex from accelerated α-particles fusing with ambient helium (Share et al. 2003a) is inconsistent with a narrow beam.

Fast neutrons from energetic ion collisions thermalize in the photosphere before being captured by hydrogen to form deuterium, which then emits a 2.223 MeV photon. *RHESSI* has made the first detailed high-resolution measurement (with the instrumental resolution at ~2 MeV of ~4 keV FWHM) of this very narrow (intrinsic width of <~0.1 keV) line (Fig. 3 in Murphy et al. 2003). The line flux, measured every 20 s, was fitted to a physically based model (Hua et al. 2002) of an accelerated ion source (whose temporal profile is given by the prompt lines) in a magnetic loop with a field perpendicular to the surface at the footpoints, taking into account pitch-angle scattering of the ions in the corona. Such a model can be used to constrain the solar ^{3}He abundance since ^{3}He will also capture neutrons, but without emitting a 2.223 MeV photon. Although reasonably good agreement can be obtained for some parameters, an improved model is needed since we know from the redshifts in the prompt lines that the field is inclined from normal to the surface.

RHESSI has provided the first direct information on the location and spatial extent of the energetic ion interaction region in a solar flare (Hurford et al. 2003). The two RMCs with 2 and 3 cm thick tungsten grids (35″ and 180″ resolution, respectively) were used to image in four energy bands for the same time interval and using the same imaging parameters: 2.218–2.228 MeV for the 2.223 MeV line, 3.25–6.5 MeV dominated by C and O γ-ray lines, and 0.3–0.5 and 0.7–1.4 MeV dominated by electron bremsstrahlung. The imaging at 180″ resolution showed that the sources in all the bands were near the optical flare.

Using both thick RMCs, the 2.223 MeV line source was determined to be less than ~1′ in size, and its centroid was found to be displaced by ~20″ ($\pm$6″) (~14,000 km) from the centroid of the 0.3–0.5 MeV (and 0.7–1.4 MeV) electron bremsstrahlung sources (Fig. 4). Models indicate that the 2.223 MeV line source should be within ~500 km (<1″) of the energetic ion interaction region (Hua et al. 2002), and thus it is a good tracer of the energetic ions. The separation of the centroids clearly implies a difference in acceleration and/or propagation between the accelerated electron and ion populations. No significant HXR emission was detected near the 2.223 MeV centroid. No significant flare Hα emission was observed at the centroid, although weak Hα emission is seen both to the east and to the west.

Flare-accelerated ions interact with the solar atmosphere to produce radioactive nuclei (and pions) that decay with the release of a positron. The positrons then slow down through Coulomb collisions and annihilate in flight, emitting two photons at 511 keV, or they capture an electron to form positronium in either the singlet or the triplet state. Annihilation from the singlet state also produces two 511 keV photons, but annihilation from the triplet state produces 3 photons with a continuum of energies up to 511 keV. The line shape and the $3\gamma/2\gamma$ ratio depend on the temperature, density, and composition of the medium where these processes take place. *RHESSI* has obtained the first high-resolution measurement of the positron annihilation line (Share et al. 2003b). The observed approximately Gaussian shape and measured width of 8.1 $\pm$ 1.1 keV FWHM are consistent with positronium formation by charge exchange in flight with neutral hydrogen at ~6000 $\pm$ 300 K or with free annihilation in a hot ~(4–7) $\times$ 10^5 K plasma. The observed upper limit to the $3\gamma/2\gamma$ ratio is only marginally consistent with the former, and the latter requires an implausibly large atmospheric column density at transition region temperatures.

7. DISCUSSION

This flare shows two clearly different acceleration and energy releases: (1) a coronal acceleration of electrons to tens of keV in the rise phase, identified here for the first time, although possibly observed before (Alexander & Metcalf 1997) but not recognized as nonthermal since high spectral resolution was not available, and (2) the more common impulsive phase acceleration that apparently is related to magnetic reconnection. Although there is a coronal source present at this time, perhaps above the loop top, it is a superhot thermal source, unlike the nonthermal source of Masuda et al. (1994).

In the rise phase, substantial numbers of electrons are accelerated in the corona with a steep double power law (electron spectrum $\delta_L = \sim 6$, $\delta_H = \sim 8$) with break energies of ~50–60 keV. Only a small fraction of these electrons reach the chromosphere; presumably most of them deposit their energy into the corona. No γ-ray line emission is detected, so there is no significant ion acceleration to tens of MeV energies.

During the impulsive phase, the accelerated electron spectrum becomes much harder, with electron power-law exponents $\delta_L = \sim$ 2.5–3.5, $\delta_H = \sim$ 4–4.5, and break energies of ~110–150 keV. Above ~500 keV, there appears to be another electron component extending to greater than 7 MeV, with a flatter spectrum. Detailed (~7″) imaging of the 0.3–0.5 MeV band (Fig. 4, *black contours*) shows that these emissions overlap the 50–100 keV HXR sources but are more concentrated toward the limb where the south footpoint, which has the flatter spectrum, is located. Thus, the electrons from tens of keV up to relativistic energies appear to be accelerated in the same regions. Preliminary timing analyses indicate that the MeV bremsstrahlung continuum may lag behind the HXR continuum by ~10 s.

The rate of energy deposition by the accelerated electrons peaks at ~10^{29} ergs s^{-1} above ~20 keV during the rise phase and drops to ~2 $\times$ 10^{28} ergs s^{-1} at the start of the impulsive phase, decreasing to below 10^{28} ergs s^{-1} by 0040 UT (Holman et al. 2003). It should be emphasized that these are lower limits to the energy in electrons. If the low-energy cutoff is 10 keV during the rise phase, the total energy (and power) in accelerated electrons would go up by about an order of magnitude.

Emslie (2003) shows that, in principle, a low-energy cutoff is not necessary for a warm plasma. Electrons with energies below ~5kT lose significantly less energy than in the cold target approximation, with the energy-loss rate dropping to zero at ~1kT. Using his formulas, we obtain ~4 $\times$ 10^{34} ergs as the upper limit to the total energy released in all accelerated electrons for $kT \sim 2$ keV. This is far more energy than ever deduced, even for the largest flares, but a larger kT would reduce this estimate significantly.

Information on the spectrum of the accelerated ions can be obtained from comparing γ-ray line fluences. This flare emitted

28.6 ± 13, 21.4 ± 4.5, 192.6 ± 4.8, and 163 ± 14 photons cm^{-2} in the C line, the Ne line, the neutron capture ^2H (2.223 MeV) line, and the 4–7 MeV band, respectively. Assuming that the accelerated ion spectrum is a single power law extending down to 2.5 MeV nucleon^{-1}, the ^2H/4–7 MeV, ^2H/Ne, and ^2H/C fluence ratios give power-law exponents of 3.4 ± 0.1, 3.8 ± 0.1, and 4.0 ± 0.5, respectively. Taking the middle value, we obtain a minimum total energy in accelerated protons above ~2.5 MeV (the threshold for the Ne line) of $\sim 1.4 \times 10^{30}$ ergs, and we obtain a minimum total energy in all accelerated ions (protons plus heavier nuclei) of $\sim 10^{31}$ ergs. Here we have assumed the cross sections and energy-loss modeling of Murphy, Kozlovsky, & Ramaty (1988), and "impulsive flare" abundances (Ramaty, Mandzhavidze, & Kozlovsky 1996) with α/proton = 0.5, α/O = 50, and $^3He/^4He = 1$; this will be checked with more detailed future analysis.

Assuming a thick target, we obtain a rate of energy deposition by energetic, $>\sim 2.5$ MeV nucleon^{-1} ions of $\sim 1.5 \times 10^{28}$ ergs s^{-1} in the first 4 minutes of the impulsive phase, dropping to $\sim 5 \times 10^{27}$ ergs s^{-1} in the following 10 minutes. Thus, a comparable amount of energy is being deposited by accelerated >2.5 MeV nucleon^{-1} ions as by accelerated >30 keV electrons during the impulsive phase.

The time history of the 3.25–6.5 MeV nuclear prompt line emission is generally similar (with a lag of ~10 s) to the 0.3–0.5 and 0.7–1.4 MeV electron bremsstrahlung bands (Fig. 1 in Hurford et al. 2003). This similarity has been seen before in other γ-ray flares, e.g., 1980 June 7 (Chupp 1990), and it suggests a common acceleration for electrons and ions. If they are accelerated and transported similarly, however, the ion-associated γ-ray source would be expected to coincide spatially with the electron bremsstrahlung source. The centroid of the 2.223 MeV line appears to be in a positive polarity magnetic region, at one foot of large-scale postflare loops (Fig. 4). The three hard X-ray footpoints and the coronal source seen in the impulsive phase are inside these large-scale loops, likely on an inner arcade of loops. One way of separating ions from electrons is by a large-scale quasi-static electric field. Another possibility, consistent with the observed delay of ~10 s of the ions relative to the electrons, is that the acceleration of the electrons and/or their subsequent interactions with the ambient medium produced a disturbance that propagated into these higher loops and accelerated the ions. Also, stochastic acceleration processes may favor shorter loops for electron acceleration (Miller 2000).

Johns & Lin (1992) showed that precise high-resolution measurements of optically thin HXR spectra can be directly inverted to obtain the spectra of the parent X-ray–producing electrons (assumed isotropic) averaged over density (also referred to as mean electron flux spectra [Brown et al. 2003] or thin-target spectra), without assumptions about physical conditions in the emission region. The precise measurements of the spatially integrated spectra provided by *RHESSI*, especially for intense flares, allow us to apply these analysis techniques for the first time. Piana et al. (2003) have devised a regularized inversion algorithm that yields the smoothest electron flux spectrum consistent with the data, while retaining real features. These results show promise, but caution must be exercised since small (of order 1%) uncertainties in the X-ray spectrum (such as those due to albedo, nonuniform target ionization, corrections for pulse pileup, etc.) can lead to large uncertainties in the inferred electron spectra.

Kontar et al. (2003) find that during the impulsive phase of this flare, the high-resolution HXR spectra deviate from a power-law behavior in a manner consistent with nonuniform target ionization. Schmahl & Hurford (2002) have shown that *RHESSI* may be able to image albedo patches. *RHESSI* is also capable of measuring the polarization of the HXRs (~20–200 keV) through scattering from a well-placed passive beryllium-scattering cylinder into the rear segments of the surrounding GeDs (Smith et al. 2002; McConnell et al. 2002), and of γ-rays (~0.15–2 MeV) through scattering directly from one GeD to another GeD (see Coburn & Boggs 2003). These measurements will provide information on the electron anisotropy. Such studies, together with other measurements (i.e., radio imaging and spectroscopy [White et al. 2003] and with optical [Firstova, Xu, & Fang 2003] polarization) will provide further constraints on the processes of energy release and particle acceleration in flares.

This research is supported in part by NASA contract NAS5-98033. *RHESSI* is named for the late Reuven Ramaty, a coinvestigator and a pioneer in the fields of solar physics, γ-ray astronomy, nuclear astrophysics, and cosmic rays.

REFERENCES

Alexander, D., & Metcalf, T. R. 1997, ApJ, 489, 442
Brown, J. C., Emslie, A. G., & Kontar, E. P. 2003, ApJ, 595, L115
Chupp, E. L. 1990, Phys. Scr., T18, 15
Coburn, W., & Boggs, S. E. 2003, Nature, 423, 415
Emslie, A. G. 2003, ApJ, 595, L119
Emslie, A. G., Kontar, E. P., Krucker, S., & Lin, R. P. 2003, ApJ, 595, L107
Firstova, N. M., Xu, Z., & Fang, C. 2003, ApJ, 595, L131
Fletcher, L., & Hudson, H. S. 2002, Sol. Phys., 210, 307
Holman, G. D., Sui, L., Schwartz, R. A., & Emslie, A. G. 2003, ApJ, 595, L97
Hua, X.-M., Kozlovsky, B., Lingenfelter, R. E., Ramaty, R., & Stupp, A. 2002, ApJS, 140, 563
Hurford, G. J., et al. 2002, Sol. Phys., 210, 61
Hurford, G. J., Schwartz, R. A., Krucker, S., Lin, R. P., Smith, D. M., & Vilmer, N. 2003, ApJ, 595, L77
Johns, C. M., & Lin, R. P. 1992, Sol. Phys., 137, 121
Kontar, E. P., Brown, J. C., Emslie, A. G., Schwartz, R. A., Smith, D. M., & Alexander, R. C. 2003, ApJ, 595, L123
Kontar, E. P., Brown, J. C., & McArthur, G. K. 2002, Sol. Phys., 210, 419
Kosugi, T., et al. 1991, Sol. Phys., 136, 17
Krucker, S., Hurford, G. J., & Lin, R. P. 2003, ApJ, 595, L103
Lin, R. P. 1974, Space Sci. Rev., 16, 189
Lin, R. P., et al. 2002, Sol. Phys., 210, 3
Lin, R. P., & Hudson, H. S. 1976, Sol. Phys., 50, 153
Makashima, K., et al. 1978, in New Instrumentation for Space Astronomy, ed. K. A. van der Hucht & G. Vaiana (New York: Pergamon), 277
McConnell, M. L., Ryan, J. M., Smith, D. M., Lin, R. P., & Emslie, A. G. 2002, Sol. Phys., 210, 125
Masuda, S., Kosugi, T., Hara, H., Tsuneta, S., & Ogawara, Y. 1994, Nature, 371, 495
Miller, J. A. 2000, in ASP Conf. Ser. 206, High Energy Solar Physics—Anticipating *HESSI*, eds. R. Ramaty & N. Mandzhavidze (San Francisco: ASP), 145
Murphy, R. J., Kozlovsky, B., & Ramaty, R. 1988, ApJ, 331, 1029
Murphy, R. J., Share, G. H., Hua, X.-M., Lin, R. P., Smith, D. M., & Schwartz, R. A. 2003, ApJ, 595, L93
Neupert, W. M. 1968, ApJ, 153, L59
Piana, M., Massone, A. M., Kontar, E. P., Emslie, A. G., Brown, J. C., & Schwartz, R. A. 2003, ApJ, 595, L127
Ramaty, R., & Murphy, R. J. 1987, Space Sci. Rev., 45, 213
Ramaty, R., Mandzhavidze, N., & Kozlovsky, B. 1996, in AIP Conf. Proc. 374, High Energy Solar Physics, ed. R. Ramaty, N. Mandzhavidze, & X.-M. Hua (Woodbury: AIP), 172

Ramaty, R., Mandzhavidze, N., Kozlovsky, B., & Murphy, R. J. 1995, ApJ, 455, L193
Schmahl, E. J., & Hurford, G. J. 2002, Sol. Phys., 210, 273
Share, G. H., & Murphy, R. J. 1995, ApJ, 452, 933
Share, G. H., Murphy, R. J., Kiener, J., & de Séréville, N. 2002, ApJ, 573, 464
Share, G. H., et al. 2003a, ApJ, 595, L85
Share, G. H., Murphy, R. J., Smith, D. M., Lin, R. P., Dennis, B. R., & Schwartz, R. A. 2003b, ApJ, 595, L89
Smith, D. M., et al. 2002, Sol. Phys., 210, 33
Smith, D. M., Share, G. H., Murphy, R. J., Schwartz, R. A., Shih, A. Y., & Lin, R. P. 2003, ApJ, 595, L81
White, S. M., Krucker, S., Shibasaki, K., Yokoyama, T., Shimojo, M., & Kundu, M. R. 2003, ApJ, 595, L111

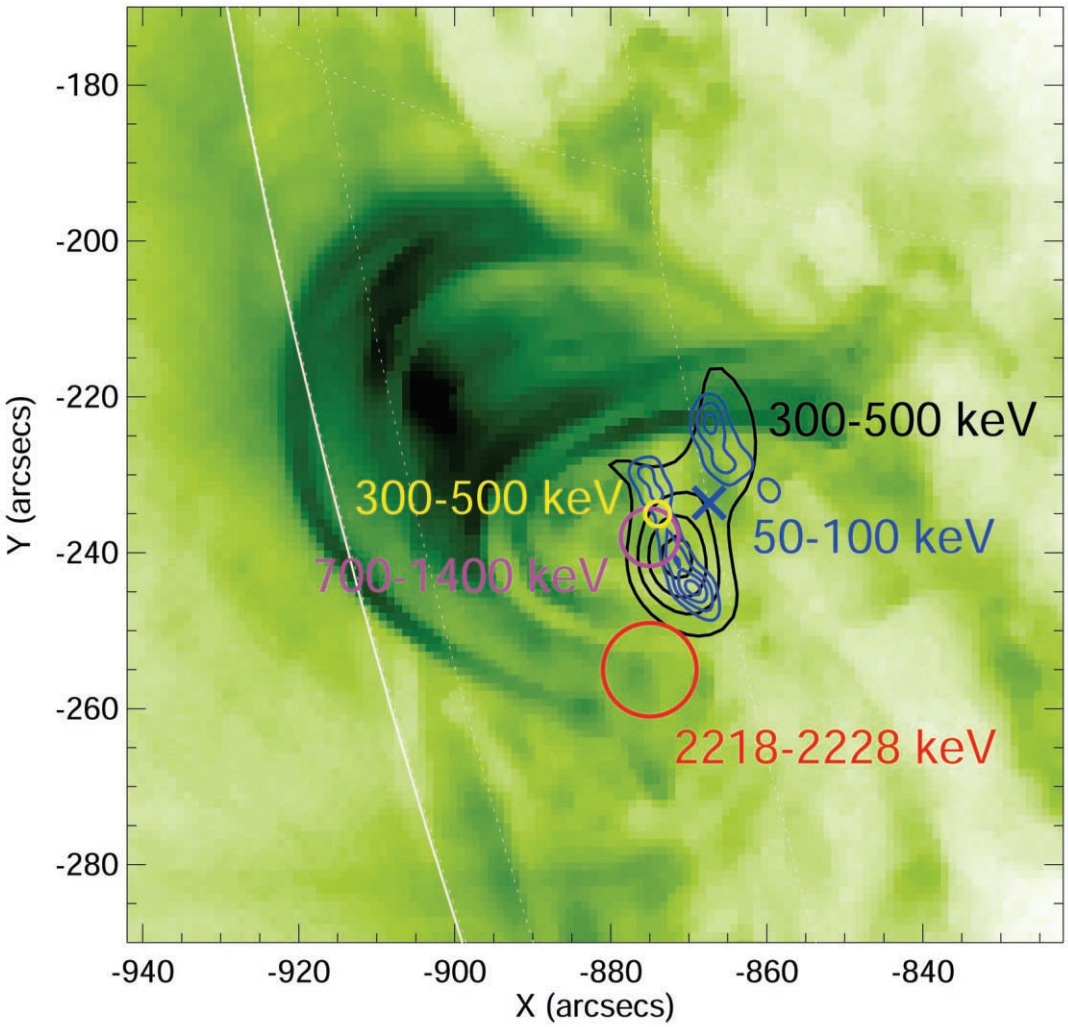

FIG. 4.—*RHESSI* centroid of the 2.223 MeV line emission (*red circle*, indicating 1 σ uncertainty) that indicates the energetic ion interaction region, superposed on a *TRACE* image taken ~90 minutes after the flare, showing the postflare loops. The yellow and pink circles are the centroids (1 σ) of the 300–500 and 700–1400 keV bands, respectively, dominated by bremsstrahlung emission. The black and blue contours show the detailed images at 300–500 and 50–100 keV, respectively; the 50–100 keV centroid is indicated by the cross.